Antiferromagnetism in a $Fe_{50}Pt_{40}Rh_{10}$ thin film investigated using neutron diffraction

D. Lott, J. Fenske, and A. Schreyer
GKSS Research Center, Max-Planck Strasse 1, 21502 Geesthacht, Germany

P. Mani and G. J. Mankey
MINT Center, University of Alabama, Tuscaloosa, Alabama 35487, USA

F. Klose
Australian Nuclear Science and Technology Organization, Menai, New South Wales 2234, Australia

W. Schmidt and K. Schmalzl
Juelich Research Center, Institute for Research on Solid State Physics, 52425 Juelich, Germany

E. V. Tartakovskaya
Institute for Magnetism, National Ukrainian Academy of Science, Vernadsky Avenue 36b, Kiev 03132, Ukraine
(Received 24 July 2008; revised manuscript received 13 October 2008; published 12 November 2008)

The temperature-dependent magnetic structure of a 200 nm thick single-crystalline film of $Fe_{50}Pt_{40}Rh_{10}$ was studied by unpolarized and polarized neutron diffractions. By applying structure factor calculations, a detailed model of the magnetic unit cell was developed. In contrast to former studies on bulk samples, our experimental results show that the film remains in an antiferromagnetic state throughout the temperature range of 10–450 K. Remarkably, it can be demonstrated that the antiferromagnetic structure undergoes a smooth transition from a dominant out-of-plane order with the magnetic moments orientated in-plane to an in-plane order with the magnetic moments orientated perpendicular to the film plane. Theoretically this can be explained by the existence of two competing anisotropy contributions with different temperature dependencies.

DOI: 10.1103/PhysRevB.78.174413 PACS number(s): 75.25.+z, 75.70.−i, 75.50.Bb

I. INTRODUCTION

FePt-based alloys are typically the material of choice for magnetic information storage media. The high magnetic moment of Fe gives a large magnetization and the large atomic number of Pt results in a high magnetic anisotropy. This combination of high magnetization and high anisotropy enables the written bits to be smaller than ever before since magnetic grains with a high magnetic anisotropy are more thermally stable.[1–3] Another desirable feature of FePt films is that the anisotropy often results in perpendicular magnetization, which is the preferred orientation for current media. Although these materials are widely used, our understanding of the fundamental physics governing the behavior of magnetization, magnetic anisotropy, and magnetic phases still mandates further inquiry. Our aim is to enhance the knowledge of these materials in order to enable the production of layered structures with a more versatile range of tunable magnetic properties.

One way to control the magnetic properties in these materials is through the introduction of a third element into the crystal matrix. When a small amount of Rh is added to replace Pt in the equiatomic alloy, new magnetic phases emerge. Bulk samples of $Fe_{50}Pt_{50-x}Rh_x$ were studied earlier by Yuasa *et al.*[4,5] who have used a pendulum-type magnetometer, x-ray diffraction, Mossbauer spectroscopy, and resistivity measurements to examine the magnetic phase diagram with regard to temperature and Rh concentration.[6–8] These measurements showed that the observed magnetic phase transitions are accompanied by anomalous changes in the resistivity, abrupt changes in the lattice parameters, and discontinuous increases in the axial ratio c/a and the cell volume V.[4–8] Three different magnetic phase transitions were observed with increasing temperature: (I) an antiferromagnetic (AF)-paramagnetic (PM) transition for $30<x<14.25$, (II) an AF-ferromagnetic (FM) transition for $14.25<x<9.5$, and (III) a FM-PM transition for $9.5<x<0$. Regime (II) is of particular interest for some potential applications due to the AF-FM phase transition, for example, thermally switchable exchange bias coupling. Exploring the details of this transition may enable us to understand better and eventually control the type of magnetic behavior exhibited by the material. In addition, it is well known that the physical properties of a thin film can differ dramatically from the bulk behavior due to dimensionality effects. With modern film deposition techniques, we now have the capability to control the crystallinity, chemical composition, and chemical ordering and we can produce thermodynamically metastable phases of unprecedented quality. In this work we present a study of the temperature dependence of the magnetic configuration of a thin epitaxial film of $L1_0$ structured $Fe_{50}Pt_{40}Rh_{10}$ by unpolarized and polarized neutron diffractions.

This paper is organized as follows. In Sec. II the characterization of the film with x-ray diffraction is presented. Section III illustrates the method of the unpolarized and polarized neutron diffractions before the experimental results of temperature-dependent neutron-diffraction measurements are presented in Sec. IV. The diffraction data are discussed in the framework of structure factor calculations in Sec. V. The latter allow a detailed model for the temperature dependence of the magnetic structures to be determined. Finally, a theo-

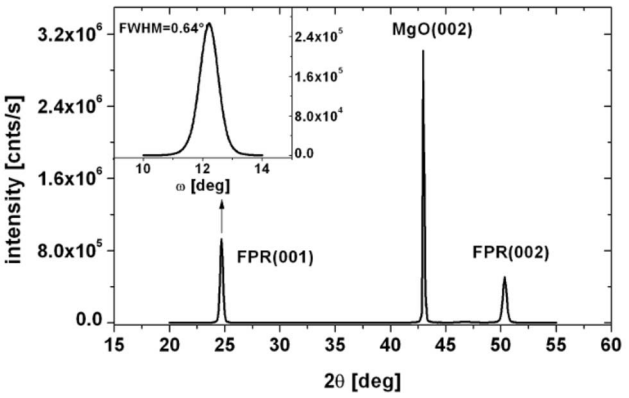

FIG. 1. Out-of-plane x-ray diffraction spectrum of a 200 nm $Fe_{50}Pt_{40}Rh_{10}$ film grown on a MgO substrate. The insert shows the rocking scan at the structural (001) Bragg peak of the film.

retical description based on the phenomenological findings is given in Sec. VI.

II. GROWTH AND STRUCTURAL CHARACTERIZATION OF THE FILM

The epitaxial $Fe_{50}Pt_{40}Rh_{10}$ alloy film was grown by magnetron co-sputtering in a UHV chamber with a base pressure of less then 1×10^{-8} mbar back filled with ultrapure Ar to a pressure of 4.5×10^{-5} mbar. Single crystal MgO(001) was used as the substrate and it was degassed at 700 °C for a few hours prior to the deposition of the layers. A layer of Cr followed by a layer of Pt was used as the seed layer combination for the growth of $L1_0$ ordered $Fe_{50}Pt_{50-x}Rh_x$ films.[9] The Cr and Pt layers have thicknesses of 3 and 12 nm, respectively. To prevent oxidation the alloy is capped with a Pt layer of 2 nm thickness. The final thickness values obtained from a quartz-crystal microbalance were cross-checked with a bilayer of Rh(10 nm)/Pt(5 nm) grown on MgO(100) under the same conditions confirming a nominal thickness of about 200 nm for the $Fe_{50}Pt_{40}Rh_{10}$.

A. X-ray characterization

The structure of the $Fe_{50}Pt_{40}Rh_{10}$ film, in particular the quality of the crystal and the chemical order of the film, was characterized by x-ray diffraction using Cu $K\alpha$ radiation at room temperature. Figure 1 shows a radial scan along the sample normal in (001) orientation of the MgO substrate and the film. Besides the strong MgO (002) substrate peak the (001) and (002) reflections from the $Fe_{50}Pt_{40}Rh_{10}$ film can be clearly observed. The appearance of the first-order peak is a signature of the chemically well ordered $L1_0$ structure of the film (see Fig. 2). If the film was chemically disordered, i.e., that all sites in the fct crystal structure were occupied by Fe or Pt/Rh atoms with the same probability, the first-order Bragg reflection would be forbidden due to destructive interference.

The degree of chemical order of the $Fe_{50}Pt_{40}Rh_{10}$ film is defined by the order parameter

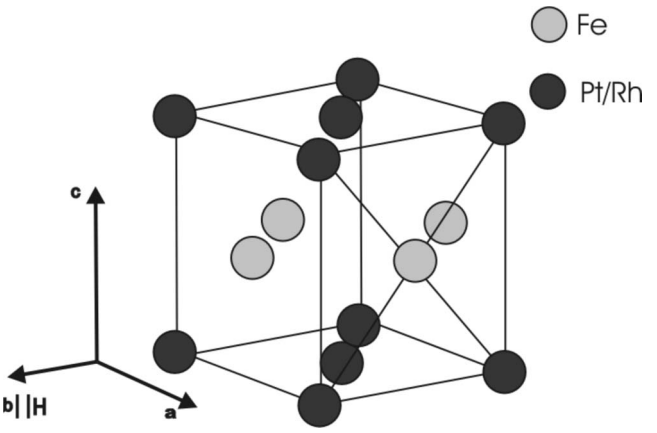

FIG. 2. Unit cell of $Fe_{50}Pt_{50-x}Rh_x$ alloys in the $L1_0$ structure.

$$S=\sqrt{\frac{I_{001}|F_{002}|^2L_p^{002}}{I_{002}|F_{001}|^2L_p^{001}}}, \tag{1}$$

where I_{hkl} is the integrated peak intensity of the corresponding Bragg reflection and L_p the Lorentz polarization correction for single crystals.[10] The structure factors are given by $F_{002}=2f_{\mathrm{av}}$ and by $F_{001}=f_{\mathrm{Pt\text{-}Rh}}-f_{\mathrm{Fe}}$ for the (001) and (002) peaks, respectively, where f_{av} is the average structure factor of the participating atoms in the unit cell and $f_{\mathrm{Pt\text{-}Rh}}$ is the weighted average structure factor of the Pt and Rh atoms in the centered tetragonal structure. For the $Fe_{50}Pt_{40}Rh_{10}$ film we calculated an order parameter of $S\approx0.95$ which is very close to perfect ordering. The small rocking curve width of 0.64° for the (001) reflection (see Fig. 1) verifies the excellent crystal orientation of the film. Using the Debye-Scherrer formula an average crystallite size of about 300 Å was extracted from the radial scans. Phi scans determine the in-plane orientation of the $Fe_{50}Pt_{40}Rh_{10}$ and MgO unit cells. Figure 3 shows the results. The fourfold symmetry of the scans confirms the epitaxial growth of the film and the offset between the MgO(220) and the $Fe_{50}Pt_{40}Rh_{10}$(011) reflections that shows the expected 45° in-plane rotation between the crystallographic axes of the film and the MgO substrate. The

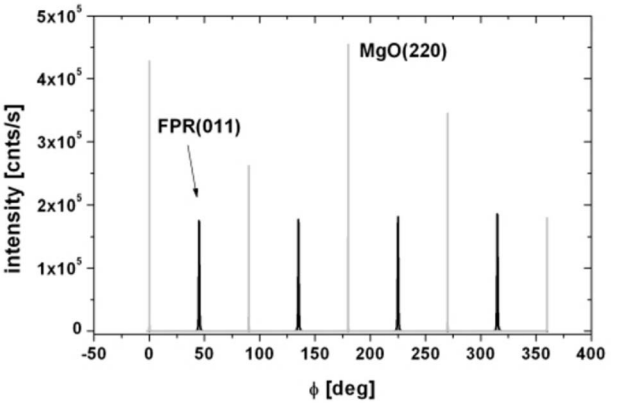

FIG. 3. Phi scans showing the $Fe_{50}Pt_{40}Rh_{10}$ (011) and MgO (220) reflections. The scans reveal a 45° offset between film and substrate.

lattice parameters of the $Fe_{50}Pt_{40}Rh_{10}$ film determined by x-ray diffraction are $a=2.750$ Å and $c=3.631$ Å for the in-plane and out-of-plane directions, respectively. These values differ only slightly from the bulk values of $a_{bulk}=2.734$ Å and $c_{bulk}=3.644$ Å, respectively.[4]

III. METHOD OF UNPOLARIZED AND POLARIZED NEUTRON DIFFRACTION

A. Unpolarized neutron scattering

Section II A illustrates how the crystal structure and chemical ordering of the thin film can be determined by x-ray diffraction. For the study of the magnetic configuration, however, a technique is needed which is also sensitive to the arrangement of the magnetic moments in the film. For this purpose, unpolarized and polarized neutron diffractions are ideally suited due to the high sensitivity of the neutrons to the magnetic structure in addition to its sensitivity to the arrangements of the atomic nuclei. The equation of the differential cross section for unpolarized neutrons can be written as

$$\left(\frac{d\sigma}{d\Omega}\right)^{\text{unpol}} = \left|\sum_j (b_j^2 + p_j^2)\exp(-i\vec{Q}\cdot\vec{r}_j)\right|^2, \qquad (2)$$

where b_j and p_j are the nuclear and magnetic scattering lengths, respectively. $\vec{Q}$ is the scattering vector and $\vec{r}_j$ the position of the jth scatterer.[11–16]

Unpolarized neutron scattering allows us to distinguish between different magnetic configurations. In particular, for AF configurations additional purely magnetic peaks appear at half order locations in the reciprocal Q space since the AF magnetic order doubles the unit cell. The determination of FM ordering by unpolarized neutron scattering is more complex. Since the unit cell of the magnetic and chemical ordering is identical in the FM case, both contributions, the nuclear and magnetic part, lead to intensities at the same Q values. Therefore FM ordering results only in changes in the scattered intensity at the position of the structural Bragg peaks and, in order to separate magnetic and structural scattering contributions, the scattered intensity has to be measured as a function of external parameters such as temperature (e.g., above and below the Curie temperature) or magnetic field (e.g., remanent versus saturated magnetic configuration).

B. Polarized neutron scattering

Direct investigation of the orientation of the magnetic spins (i.e., at a particular temperature and magnetic-field setting) requires the use of polarized neutrons and polarization analysis of the scattered beam. The most simple polarization analysis technique is called unidirectional neutron polarimetry.[17] In this method the sample is exposed to a unidirectional magnetic field. Depending on the different polarization states of incoming and scattered-neutron beam, four cross sections for the magnetic part of the scattering intensity are distinguished given by the two possible states for the incident and scattered neutrons, respectively, leading to + +, − −, − +, and + − intensity channels.[15] The symbols + and − denote the neutron spin being parallel or antiparallel, respectively, to its quantization axis which is determined by the direction of the magnetic field at the sample. In principle two scenarios are discriminated. In the first, the spin states of the incident and scattered neutrons are identical. This scattering is called the non-spin-flip (NSF) scattering channel. Here, only those components of the magnetic moments which are parallel (+) or antiparallel (−) to the guide field direction contribute to the signal. For any magnetic state with nonzero net magnetization (e.g., FM configuration) with components of the magnetic moments along the guide field direction, the intensities for the two NSF scattering channels are different. Neutron scattering from magnetic moments oriented perpendicular to the guide field as well as perpendicular to the scattering vector Q results in a spin-flip (SF) of the neutrons during scattering. The spin-flip scattering signal is purely of magnetic origin and usually both spin-flip channels have the same intensities. Some specific magnetic configurations, e.g., helicoidal configurations, lead to an intensity difference in the two spin-flip channels. It is important to note that nuclear scattering contributes equally to both NSF channel intensities but does not contribute to the intensity of the SF channels.

Due to the high crystalline order it is possible to conclude the following: since only the magnetic moments that are oriented perpendicular to the scattering vector Q are observable, it is necessary to measure Bragg peaks along different Q directions (e.g., perpendicular directions) in order to gain a three-dimensional image of the magnetic configuration. In the present case the scans are carried out along the out-of-plane {001} and the in-plane {100} directions. Since the {100} and {010} directions are crystallographically identical, it is sufficient to restrict the measurements to one in-plane direction.

Magnetic contributions at Bragg reflections of different orders are due to different types of magnetic ordering. In general, it is evident that half order reflections are a signature of an AF configuration due to the doubling of the unit cell. It is also well understood that the second-order Bragg reflections are sensitive to contributions with a nonzero net magnetic moment, e.g., FM ordering. However, for first-order reflections a more sophisticated analysis may be necessary depending on the particular crystalline structure, e.g., on the number and position of the atoms in the unit cell. By applying structure factor calculations (see Appendix) it can be shown that for the fct ordered $Fe_{50}Pt_{40}Rh_{10}$ film magnetic contributions to the out-of-plane (001) Bragg peak are due to complete or partial FM ordering with the magnetic moments oriented perpendicular to the {001} direction. Besides the magnetic intensity, nuclear scattering which is proportional to the difference of the nuclear scattering lengths between Fe and the concentration averaged Pt/Rh also contributes to the first-order out-of-plane reflection. Since these are very similar [Fe: 9.45 fm (80% Pt/20% Rh) and 8.86 fm], the nuclear scattering part is very weak.

In sharp contrast, structure factor calculations show that the (100) Bragg-peak intensity originates solely from an in-plane AF ordering of the Fe moments. This can be explained by two equivalent Fe sites contributing to the (100) Bragg reflection being 180° out of phase and canceling each other

TABLE I. Nuclear (N) and FM/AF magnetic contributions to the in-plane (100)/(010) and out-of-plane (001) Bragg-peak intensities of $L1_0$ structured $Fe_{50}Pt_{40}Rh_{10}$.

Order	{100}	{010}	{001}
$\frac{1}{2}$	AF	AF	AF
1	AF	AF	N+FM
2	N+FM	N+FM	N+FM

for any nuclear or ferromagnetic contributions. Table I summarizes the results of the structure factor calculations of the $L1_0$ thin film.

IV. NEUTRON-DIFFRACTION MEASUREMENTS

The neutron-diffraction measurements were carried out at the POLDI instrument at the GKSS Research Center in Geesthacht and at the triple axis cold neutron spectrometer IN12 at the ILL in Grenoble. POLDI is a two-axis diffractometer using a PG(002) monochromator and a velocity selector for $\lambda/2$ suppression. A wavelength of 1.8 Å was used for the unpolarized neutron-diffraction measurements. IN12 is a three axis spectrometer and uses a PG(002) vertically focusing monochromator. In our experiments we used IN12 in elastic mode, i.e., as a diffractometer. IN12 uses a supermirror bender as polarizer. The wavelength for the experiments was set between 4.18 and 5.2 Å and a Be filter was used for the $\lambda/2$ suppression. A curved Heusler(111) monochromator is used for the polarization analysis.

A. Unpolarized neutron diffraction

In the unpolarized neutron measurements scattering intensities were observed at the half-, first-, and second-order Bragg peaks of the $L1_0$ structured $Fe_{50}Pt_{40}Rh_{10}$ thin film along both the out-of-plane {001} and the in-plane {100} directions. Their integrated intensities corrected for sample illumination, Q dependence of the magnetic form factor, and normalized by beam monitor intensities are plotted in Fig. 4. All three AF peaks, $(00\frac{1}{2})$, $(\frac{1}{2}00)$ and (100), show strong temperature dependence. At low temperature the AF order due to the out-of-plane $(00\frac{1}{2})$ peak is dominant while the in-plane contribution of an AF order at $(\frac{1}{2}00)$ is considerably weaker. Both AF half-order intensities decrease with increasing temperature. By fitting the graphs with a power law of the form $\sqrt{I(T)}=(1-T/T_N)^{\beta}$ with T_N denoting the AF transition temperature and β the critical exponent, it can be shown that the in-plane order vanishes at about $T_N=250$ K before the out-of-plane order, which disappears at about 320 K (see Fig. 4). The critical exponents β for both half-order reflections are fitted to a value of 0.2 indicating that the observed transitions are of the second kind. In addition to the $(\frac{1}{2}00)$ reflection, another AF in-plane peak was observed at the (100) Bragg position. This also showed a strong variation in temperature. In contrast to the half-order reflections its intensity increased from low temperatures to a maximum signal at around $T=300$ K before it decreased again and vanished at around $T=450$ K.

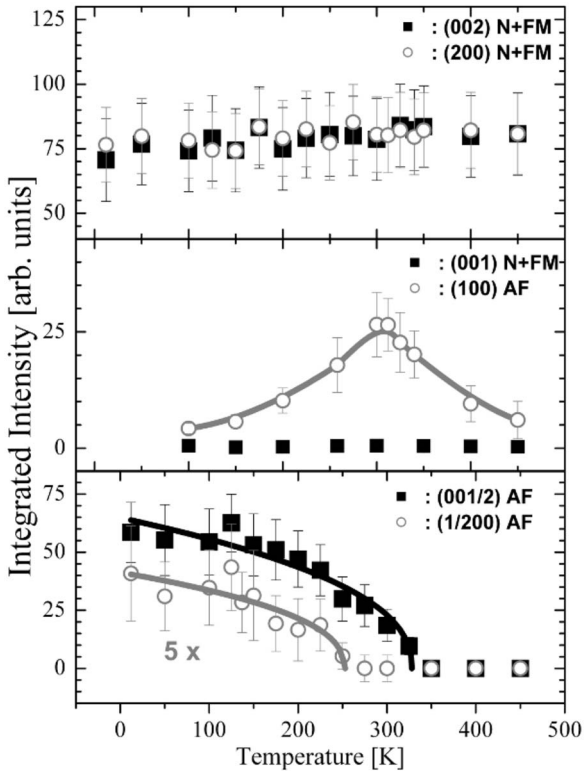

FIG. 4. Temperature dependence of the integrated neutron-diffraction intensity at three in-plane (200), (100), $(\frac{1}{2}00)$ (open circles) and three out-of-plane (002), (001), $(00\frac{1}{2})$ reflections (solid squares). The intensity of the $(\frac{1}{2}00)$ reflection was multiplied by a factor of 5 in the lower panel. The line of the (100) AF peak is a guide for the eyes. The lines for the $(00\frac{1}{2})$ (black line) and $(\frac{1}{2}00)$ (gray line) peaks are fits (for further details see text).

The intensities of the first- and second-order out-of-plane Bragg peaks (001) and (002), as well as the in-plane (200) peak, can potentially have contributions from FM order (see Table I) but within the investigated temperature range these reflections show constant values in their integrated intensities (within error). Since the appearance or disappearance of any FM order should be linked with changes in the intensity of these peaks it can be concluded that no change in the FM order is observed in the whole temperature range and the magnetic ordering in the thin film is purely of AF origin. The temperature dependence of the in-plane and out-of-plane Bragg peaks that we observed on the thin-film sample is not consistent with the AF-FM transition that was observed in bulk crystals.[4,5,8] Instead, the data presented in Fig. 4 clearly show a temperature-driven transition from an out-of-plane to an in-plane AF order (a more detailed explanation will be given below). Apparently, this reorientation transition of the AF structure starts at low temperature and is completed at around $T=330$ K. From about $T=300$ K the magnetic intensity of the AF in-plane order decreases with increasing temperature and finally the AF magnetic ordering vanishes above $T=450$ K.

From the Q values of the (200) and (002) Bragg peaks the in-plane and out-of-plane lattice parameters, a and c, respectively, can be determined for the thin film. Their dependence

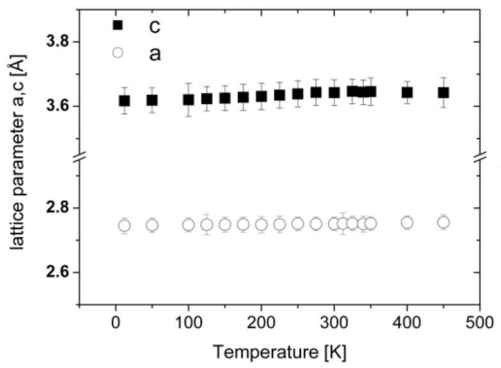

FIG. 5. The variation in the lattice parameters a and c with temperature.

on the temperature is plotted in Fig. 5. While the in-plane lattice parameter a is constant within the measured temperature range, there is a small continuous change in the lattice parameter c again indicating that the film differs significantly from the bulk state in which the AF-FM transition was accompanied by a sudden shift in the lattice parameters.[4] The restricted in-plane lattice expansion may be due to the epitaxial clamping of the film to the substrate which may be the underlying cause of why the magnetic behavior of the film differs from the bulk material.

In addition to the unpolarized neutron-diffraction measurements along the {100} and {001} directions, supplemental data sets were recorded at the (110) and $(\frac{1}{2}\frac{1}{2}0)$ Bragg reflexions. While a weak but constant intensity was observed at the (110) peak, no intensity could be detected at the corresponding half-order peak indicating that neither FM nor AF magnetic order was present along the {110} direction.

B. Polarized neutron diffraction

In order to obtain more detailed information on the actual orientation of the magnetic moments in the $Fe_{50}Pt_{40}Rh_{10}$ film, we performed polarized neutron-diffraction experiments with polarization analysis. The signals from thin-film samples are very weak. Even though the experiment was performed at the high neutron flux cold triple axis spectrometer IN12 at the ILL in Grenoble which, due to the use of its energy-filtering monochromator on the secondary side of the instrument, usually has very low background noise, the experiments are still very time consuming due to the small amount of material (the film has only 5 μg of material). Since no FM intensities were observable in the unpolarized experiments, polarized neutron diffraction with polarization analysis was carried out only for the AF $(00\frac{1}{2})$, $(\frac{1}{2}00)$, and (100) Bragg peaks. Since all magnetic reflections considered here are of AF origin, it is sufficient to restrict the measurements to one SF and one NSF channels. For selected scans it was confirmed that both SF (i.e., $+\rightarrow-$ and $-\rightarrow+$) and both NSF (i.e., $+\rightarrow+$ and $-\rightarrow-$) scattering channels show no differences within the error bars.

Figure 6 shows the polarized neutron intensities of the purely magnetic $(00\frac{1}{2})$, $(\frac{1}{2}00)$, and (100) AF Bragg peaks at $T=150$ K and $T=300$ K (at 300 K the $(\frac{1}{2}00)$ reflection does

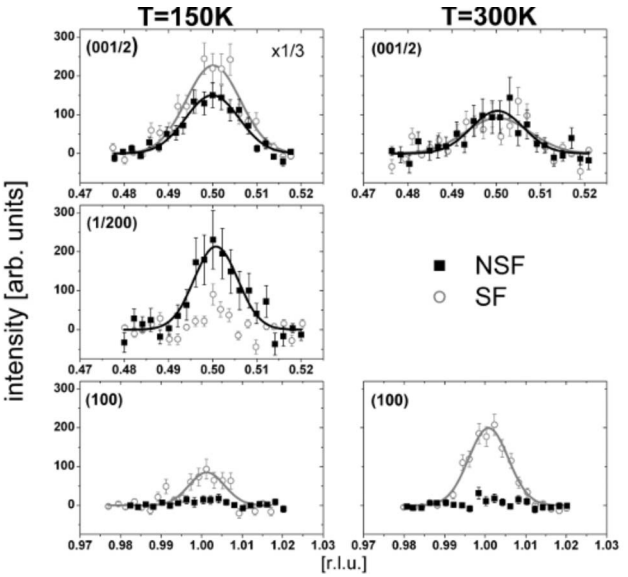

FIG. 6. Polarized neutron-diffraction scans of the $(00\frac{1}{2})$, $(\frac{1}{2}00)$, and (100) AF reflections at 150 and 300 K plotted against the individual reciprocal-lattice units (RLUs). The data sets of the $(00\frac{1}{2})$ reflection have been multiplied by a factor of 1/3.

not exhibit intensity and is therefore omitted, compare Fig. 5). A small guide field which provides the spin-quantization axis for the polarized neutrons was oriented in plane along the {010} direction. All scans are corrected for background noise and normalized to the incident-beam monitor.

At the lower temperature of $T=150$ K, the dominant $(00\frac{1}{2})$ reflection has both NSF and SF contributions with the latter being slightly more intense. The presence of both NSF and SF intensities indicates that magnetic components along the guide field direction {010} as well as along the perpendicular in-plane {100} direction contribute to the AF ordering.

For the in-plane half-order reflection $(\frac{1}{2}00)$ only the NSF channel is observed as it is expected for an AF ordering with the sublattice magnetization vectors along the {010} direction. The almost vanishing SF intensity indicates that no significant component of the sublattice magnetization vector exists along {001} contributing to this in-plane component.

The polarized neutron scattering intensities at the AF (100) peak complete the picture of the magnetic ordering at low temperatures. For this reflection only the purely magnetic SF intensity is observed. Since the guide field was oriented along the {010} direction, we can conclude that the magnetic moments contributing to the (100) order are strictly orientated along the out-of-plane direction. Summarizing the results of the polarized neutron diffraction on the three AF reflections it can be concluded that AF ordering exists in all three crystallographic directions. The half-order peaks are sensitive to the in-plane components of the sublattice magnetization vector, while the first-order in-plane (100) reflection is only due to moments oriented strictly along the out-of-plane direction of these vectors.

For higher temperatures at around $T=300$ K, only the AF ordering represented by the $(00\frac{1}{2})$ and (100) reflections remain with the latter being now the dominant contribution.

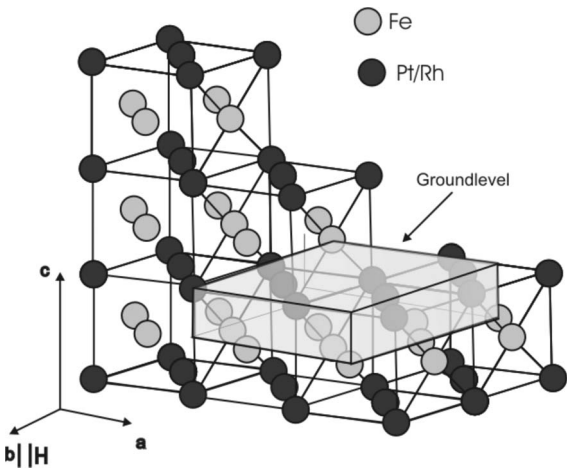

FIG. 7. Geometry of the $L1_0$ structured $Fe_{50}Pt_{40}Rh_{10}$ film. In c direction the film build a natural multilayer with alternating planes of Fe atoms (gray) and Pt/Rh atoms (black). The light gray rectangular block contains the atoms that contribute to the part of the extended unit cell which is denoted as the ground level in a two-dimensional view (see Fig. 9).

The intensity of the (100) Bragg reflection is still completely SF scattering, i.e., the magnetic components are purely oriented along the {001} direction. For the weaker $(00\frac{1}{2})$ peak the SF intensity is now comparable to the NSF intensity indicating that approximately equal amounts of sublattice magnetization components along the {100} and {010} directions are contributing to the scattering at the $(00\frac{1}{2})$ position.

V. STRUCTURE FACTOR CALCULATION AND DISCUSSION

The experimental results of the unpolarized and polarized diffraction data reveal detailed information about the magnetic ordering in the $Fe_{50}Pt_{40}Rh_{10}$ film and the orientations of the magnetic moments contributing to each of the AF Bragg peaks. By developing qualitative and quantitative structure factor calculations it is possible to reconstruct the temperature-dependent magnetic configuration of the film. The structure factor calculations are crucial for restricting the number of possible magnetic configurations. It not only confirms the existence or absence of the observed magnetic reflections but also allows one to estimate the individual contributions of each magnetic configuration for comparison to the experimental data. To explain the results including the magnetic configuration, the unit cell of the $L1_0$ crystal structure has been extended, as is illustrated in Fig. 7, to include 16 Fe and 16 Pt/Rh sites. Models were developed by structure factor calculations and take all the experimental information properly into account.

The $(\frac{1}{2}00)$ reflection is due to a doubling of the unit cell along the a axis. This reflection is observable only at low temperatures ($T<250$ K) and shows a distinct temperature dependence (Fig. 4). Therefore, it must be of magnetic origin. Since only the NSF channel shows intensity (Fig. 6), the $(\frac{1}{2}00)$ reflection is caused by components of the magnetic moments parallel or antiparallel to the b axis ($b\|H$) which

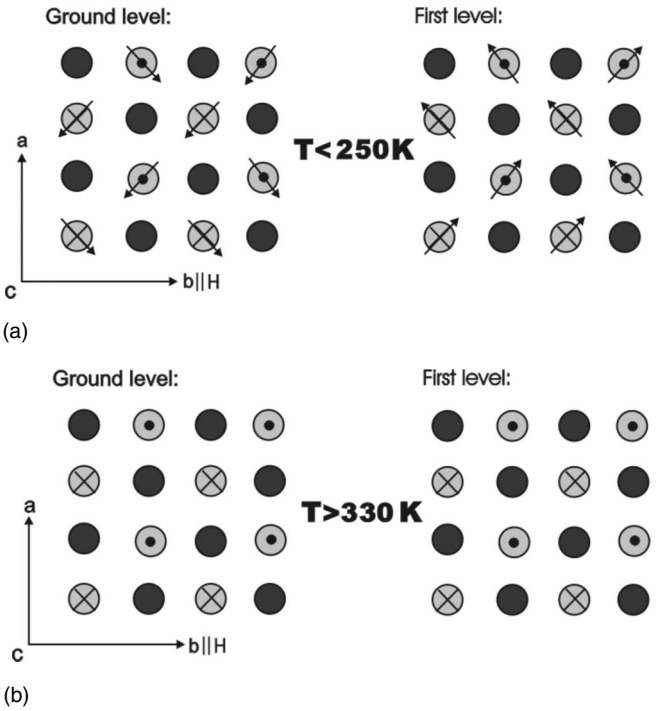

FIG. 8. Models of the magnetic configuration at low temperatures $T<250$ K and $T>330$ K for the ground and first level of the extended unit cell (see Fig. 7). The gray circles represent Fe atoms and the black circles Pt/Rh atoms. The latter are located $(1/2)c$ shifted along the c axis with respect to the Fe atoms. For $T<250$ K, the magnetic moments are tilted with respect to the a and b axes as shown by the arrows. Note the slight twists of the moments about the c axis. The dots and the crosses indicate that components of the magnetic moments are pointing up or down, respectively. The ground and first level are shifted in c direction about the distance between two Fe-atoms in this direction.

form an antiferromagnetic structure along the a axis direction.

Due to its temperature dependence, the $(00\frac{1}{2})$ reflection can also be identified as resulting from an AF arrangement of magnetic-moment components in the c axis direction. Since both SF and NSF intensities are present, the direction of these moment components must be at about 45° with the a and the b axes.

The AF (100) reflection shows its highest intensity at about 300 K and decays toward higher and lower temperatures. The intensity is solely SF. Therefore, the AF periodicity along the a direction must result from moment components which are parallel or antiparallel to the c axis. Figure 8 shows the proposed magnetic configurations at low and high temperatures, respectively. Considering the enlarged unit cell the structure factor calculations give the following expressions for the structure factors $F_{\vec{Q}}$ for the different reflections (for details, see Appendix):

$$F_{0\ 0\ 1/2} = 16 p_{\mathrm{Fe}} \cos(\alpha), \tag{3a}$$

$$F_{1/2\ 0\ 0} = 8 p_{\mathrm{Fe}} \sin(\alpha), \tag{3b}$$

$$F_{0\ 1/2\ 0} = 0, \tag{3c}$$

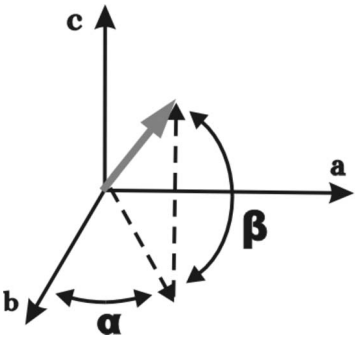

FIG. 9. Orientation of the magnetic moment in the $Fe_{50}Pt_{40}Rh_{10}$ film. Here α is the angle to the in-plane a axis and β is the angel to the out-of-plane c axis.

$$F_{1/2\ 1/2\ 0} = F_{1/2\ 0\ 1/2} = F_{0\ 1/2\ 1/2} = 0, \tag{3d}$$

$$F_{001} = 16(b_{\mathrm{Fe}} - b_{\mathrm{Pt\text{-}Rh}}), \tag{3e}$$

$$F_{100} = F_{010} = 16 p_{\mathrm{Fe}} \sin(\beta), \tag{3f}$$

$$F_{002} = F_{200} = F_{020} = 16(b_{\mathrm{Pt\text{-}Rh}} + b_{\mathrm{Fe}}). \tag{3g}$$

The parameters α and β denote the orientation of the magnetic moment with respect to the axis of the unit cell and describe the in-plane and out-of-plane angles (see Fig. 9). Since the crystallographic structure along both in-plane directions is in principle interchangeable and no external force is applied to break the in-plane symmetry, four different domains following the fourfold in-plane symmetry are of equal probability. They can be imagined as the magnetic structure shown in Fig. 8 with the magnetic configuration in each plane turned by 90°, 180°, and 270°. In the following, the four domains will be denoted as parallel or perpendicular domains depending on their orientation of the magnetic configuration with respect to the one depicted in Fig. 8. Assuming that each domain contributes equally to the scattering signal, the observed intensity can be calculated from the sum over all four domains. It is important to note that for the perpendicular domains, the contributions to the $(00\frac{1}{2})$ and (100) peaks do not change, but the intensities observed for the $(\frac{1}{2}00)$ peaks are now in the $(0\frac{1}{2}0)$ channels. Furthermore only the magnetic components perpendicular or parallel to the guide field contribute to the $(00\frac{1}{2})$ peak (SF) for the parallel or perpendicular domains, respectively, leading to only SF for the parallel and NSF for the perpendicular domains. The ratio between the intensities at the $(00\frac{1}{2})$ and $(\frac{1}{2}00)$ peaks using the structure factor calculation is given by

$$\frac{I_{1/2\ 0\ 0}}{I_{0\ 0\ 1/2}} = \frac{(F_{1/2\ 0\ 0})_{\parallel}^2 + (F_{1/2\ 0\ 0})_{\perp}^2}{(F_{0\ 0\ 1/2})_{\parallel}^2 + (F_{0\ 0\ 1/2})_{\perp}^2} = \frac{64|p_{\mathrm{Fe}}|^2 \sin^2\alpha}{(2)256|p_{\mathrm{Fe}}|^2 \cos^2\alpha} = \frac{1}{8}\tan^2\alpha, \tag{4}$$

with the suffices $\parallel$ and $\perp$ denoting the parallel and perpendicular domains, respectively. It demonstrates that the in-plane angle α can be calculated by knowing the ratio between both half-order intensities. Similarly the out-of-plane angle β can be estimated by comparing the half-order reflections with the first-order in-plane reflection,

$$\frac{I_{1\ 0\ 0}}{I_{0\ 0\ 1/2} + 4I_{1/2\ 0\ 0}} = \frac{(F_{1\ 0\ 0})^2}{(F_{0\ 0\ 1/2})^2 + (2F_{1/2\ 0\ 0})^2} = \sin^2\beta, \tag{5}$$

From the data it is also possible to study the behavior of the absolute value of the AF magnetization components of the sample and can be plotted by considering the different contributions to the half- and first-order reflections,

$$M = \sqrt{M_{\parallel}^2 + M_{\perp}^2} \propto \sqrt{(I_{0\ 0\ 1/2} + 4I_{1/2\ 0\ 0})^2 + I_{1\ 0\ 0}^2}, \tag{6}$$

where $M_{\parallel}$ and $M_{\perp}$ denote the components of the AF aligned magnetic moments orientated in plane and out of plane, respectively. Figure 10 shows the graphs for the total magnetization and for both the in-plane and the out-of-plane angles as a function of temperature, as determined from our experimental results. Here, the in-plane angle α shows very little variation at low temperatures and is close to 45° within the error bars. At around $T=250$ K it undergoes a rapid transition to 0° as the intensity of the half-order of the in-plane reflection vanishes. Contrary to this, a rather smooth transition is observed for the out-of-plane angle β from very little canting at low temperature. As the temperature approaches the reorientation point the canting of the AF aligned moments to the out-of-plane direction changes rapidly and finally reaches the perpendicular state at around $T=330$ K.

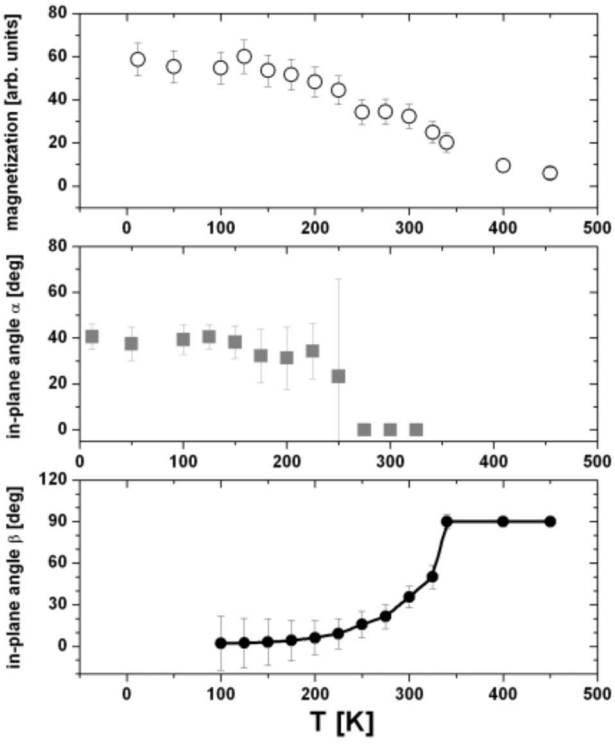

FIG. 10. Total magnetization due to the (a) AF ordering, (b) in-plane angle α, and (c) out-of-plane angle β as a function of temperature.

VI. THEORETICAL DESCRIPTION AND DISCUSSION

Due to their interesting physical properties and their potential for applications, both FePt and FeRh alloys attracted significant scientific interest. As shown by experimental work and by first-principles calculations, bulk FeRh compounds in the concentration around the equiatomic composition exhibit a temperature driven FM-AF phase transition.[18–20] In both phases the magnetic moments of the Fe atoms are orientated in plane without any considerable crystallographic anisotropy. This allows one to consider FeRh as a good material for longitudinal anisotropy devices, as well as for ultrafast laser-induced phase transformation.[21,22] On the other hand, FePt is one of the most promising candidates for perpendicular anisotropy devices like perpendicular magnetic storage media due to its large easy-axis out-of-plane anisotropy. It was shown by first-principles calculations that the Pt component is responsible for the perpendicular anisotropy in the FePt system.[23,24] The interesting question arising is what kind of anisotropy is responsible for the magnetic transitions or spin reorientations in $Fe_{50}Pt_{50-x}Rh_x$ compounds. The results presented above on the 200 nm thin film with a Rh concentration of 10% clearly show that it differs significantly from the corresponding bulk alloy systems

The smooth transformation between the two AF states with temperature can be explained on the basis of a phenomenological model which takes into account both twofold and fourfold anisotropies. The twofold anisotropy is well known for magnetic $L1_0$ structured systems as a strong anisotropy due to the easy axis. Especially for FePt compounds, the easy-axis term in the total energy plays an important role and is referred as magnetic-anisotropy energy (MAE), $E_{\mathrm{MAE}}=-K_1 m_z^2$ where $K_1>0$ is the easy axis anisotropy constant with $m_x=|m|\sin\theta\cos\varphi$, $m_y=|m|\sin\theta\sin\varphi$, and $m_z=|m|\cos\theta$, the components of the magnetization m with θ and φ denoting the angles for spherical coordinates. The fourfold anisotropy term in cubic symmetry is proportional to the fourth order of the magnetization and is given by the cubic energy term of $E_{\mathrm{KUB}}=K(m_x^2m_y^2+m_z^2m_y^2+m_z^2m_x^2)$. In the tetragonal $L1_0$ phase, the expression for the fourfold anisotropy has to be modified according to the tetragonal case,

$$E_{\mathrm{tetr}}=-[4K_2m_x^2m_y^2+K_3(m_z^2m_y^2+m_z^2m_x^2)]. \tag{7}$$

For the $L1_0$ structured thin film of $Fe_{50}Pt_{40}Rh_{10}$ the experimental results show strong evidence that the magnetic moments are canted at low temperatures. This can only be attributed to the competition between both anisotropy terms described above. As proven by first-principles calculations for FePt in accordance with recent experiments on the temperature dependence of uniaxial MAE, the origin of the easy-axis term can be described as an anisotropic exchange mediated by the induced Pt atomic spin moments, whereas the contribution from Fe is of opposite sign (i.e., easy plane) but much smaller by value. We assume that in FePtRh the origin of MAE should be the same. As it concerns the fourfold tetragonal anisotropy term (7), to our knowledge its origin has not been analyzed by first-principles calculations for the present time and should be the subject of future investigations. It is important to note that for FePt the twofold anisotropy is the dominant term leading to an alignment of the magnetic moments along the z axis. Obviously the substitution of 20% of the Pt atoms by Rh results in a drastic change at low temperature. Considering that FeRh systems do not establish considerable easy-axis anisotropy,[18] the reduced MAE may be attributed to the presence of Rh in the $Fe_{50}Pt_{40}Rh_{10}$ film.

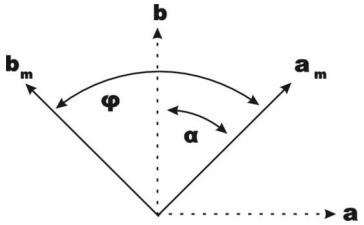

FIG. 11. The relation between the angles α and φ. The axes a and b describe the crystallographic orientations with respect to the {100} and {010} directions while a_m and b_m denote to the principal axes of the magnetization in the sample at low temperatures.

The competition between both anisotropy terms described above leads to the well-known "canted" spin structure[25] with $\cos 2\theta=\frac{K_1}{K_3}$ if $|\frac{K_1}{K_3}|<1$ and $\varphi=0°$ if $K_2<0$. Here, polar and azimuthal angles which describe the orientation of the magnetic moment are connected with the previously introduced angles β and α by the relations $\varphi=\alpha+45°$ and $\theta=90°-\beta$ (see Fig. 11). Note, that just by assuming $K_2<0$, the minimum of the energy leads to $\varphi=0°$, i.e., $\alpha=45°$ in accordance with the experimental findings for low temperatures.

It follows that the temperature dependence of the polar angle θ is connected with the temperature dependencies of the anisotropy constants K_1 and K_3. Much attention was paid to this subject for decades. In general, the temperature dependence of an anisotropy constant $K(T)$ is parametrized in a power-law dependence on the magnetization $m(T)$, namely, $K(T)\sim m(T)^n$. The first *ab initio* calculations by Callen and Callen[26] give $n=3$ for uniaxial and $n=10$ for cubical constants. The latest calculations for the interpretation of more recent experiments[21,22,27,28] gave the results of $n\sim 2$ for the uniaxial constant and $n=4$ for the cubical constant in the vicinity of the critical temperature.[23,24,29–31] In consideration of these results, it can be concluded that the twofold MAE anisotropy constant reduces much more slowly than the fourfold (cubic or tetragonal) anisotropy constants with decreasing magnetic moment of the Fe atoms.[29]

The calculations above, the experimentally observed transitions, and the phenomenological models of the magnetization deduced from neutron-diffraction measurements can be interpreted as the follows: for low temperatures the reduction in the MAE by the partial substitution of Pt atoms by Rh leads to a situation where condition $|\frac{K_1}{K_3}|<1$ is fulfilled which results in a canted phase. With increasing temperature all anisotropy constants decrease, but the fourfold anisotropy constants decrease much faster.

On the basis of the experimental results it needs to be assumed that the smallest anisotropy constant K_2 shows the fastest decrease. In the vicinity of the in-plane AF to out-of-plane AF transition and over a short temperature interval, K_2

drops already to zero while the condition $|\frac{K_1}{K_3}|<1$ is still fulfilled. The magnetic moments are still canted along the out-of-plane direction, but the part of the in-plane anisotropy which leads to $\alpha=45°$ vanishes. As experimentally observed, at around the temperature $T=330$ K the direction of AF order changes from a dominant out-of-plane to a dominant in-plane order. Around that transition, K_1 is equal to K_3 while for higher temperatures K_1 is finally dominant. At this stage the ground state of magnetization develops a magnetic configuration with an out-of-plane orientation of magnetic moments, i.e., the energy is minimized when $\theta=0°$. In the vicinity of this reordering of the AF orientation one obtains $\theta\sim\sqrt{\frac{1}{2}(1-\frac{K_1}{K_3})}$. The square dependence allows us to assume that the angle θ plays here the role similar to the one of the phase-transition parameter in a second-order phase transition.

In order to explain the low-temperature noncollinear magnetic structure and, in particular, the orientation of the in-plane components, a strict analysis of nonlocal two-ion interactions in the system such as exchange forces and two-ion anisotropies must be carried out.[24,32,33] It was shown for both FePt and FeRh that the exchange interactions due to the presence in the system of both itinerant 5*d* and local-moment 3*d* components have anisotropic and long-range behavior.[23,24,30] In a future step we intend to use these approaches for the experimental and theoretical analysis of nonlocal interactions in $Fe_{50}Pt_{50-x}Rh_x$ systems as a function of the Rh content *x*. This is out of the scope of this paper and will be presented elsewhere.

VII. CONCLUSIONS

In summary we have investigated the structural and magnetic properties of an epitaxial thin film of $Fe_{50}Pt_{40}Rh_{10}$ by means of x-ray diffraction and neutron diffraction and analyzed the results by means of detailed structure factor calculations. Contrary to earlier reports on bulk samples with the same Rh concentration, the thin film is AF ordered throughout the whole temperature range up to $T=450$ K before it becomes paramagnetic. Unpolarized and polarized neutron diffractions allow one to distinguish between the different AF orders in the film. At low temperature the ordering is dominantly out of plane with the magnetic moments oriented in plane at an angle close to 45° with respect to the in-plane *a* and *b* axes. At higher temperatures above $T=330$ K, the AF order is purely in plane with its magnetic moment oriented out of plane. The rotation of the magnetic moments from the in-plane to the out-of-plane orientation can be described in a theoretical model taking into account two major contributions to the anisotropy constants. One favors the easy axis anisotropy while the other accounts for the tetragonal anisotropy. The competition between both contributions leads to a relatively smooth transition as it is observed in the experimental data. Contrary to this, the in-plane angle, being constant close to 45° for low temperatures, undergoes a rapid transition at around $T=250$ K and aligns along the crystallographic in-plane axes for higher temperature. This first-order type of transition is also included in the theoretical description and can be attributed to the different dependencies of the anisotropy constants on the magnetization of the sample.

The intriguing behavior of the magnetic configuration investigated in this paper demonstrates that the magnetic properties of the $Fe_{50}Pt_{50-x}Rh_x$ alloy depend not only strongly on the Rh concentration but also on the thin-film state of the sample and its rigid contact to the substrate. In particular, it was shown in this paper that the magnetic properties of FePtRh alloy differ for a thin film drastically from its bulk behavior. This may open up new ways to modify the magnetic properties of this alloy to tailor them for future applications.

In continuation of this work the $Fe_{50}Pt_{50-x}Rh_x$ system will be systematically investigated with respect to these parameters. It should be noted that the detailed atomic level identification of AF or FM configurations in thin films (or bulk samples) is impossible for standard magnetic investigation tools such superconducting quantum interference device (SQUID) or other magnetometers. The comprehensive study here demonstrates that, due to their extraordinary magnetic sensitivity, unpolarized and polarized neutron diffractions are indispensable tools for investigating magnetic properties. Even for thin films where the amount of sample material is extremely small, it provides unique insights into the nature of magnetic ordering in reduced dimensionality systems.

ACKNOWLEDGMENT

The authors kindly acknowledge enlightening discussions with Margaret Elcombe. This project was supported by U.S. Department of Energy through Grant No. DE-FG02-02ER45966 and National Science Foundation Materials Research Science and Engineering Center program through Grant No. DMR-0213985.

APPENDIX: STRUCTURE FACTOR CALCULATION

The crystal structure of the $L1_0$ structured FePtRh thin film includes two different sites of Fe and Pt/Rh as illustrated in Fig. 2. Of the Pt atoms 20% are substituted by Rh atoms in random fashion. For the scattering process and the structure calculations these sites can be described as being occupied by, on average, 40/50 Pt and 10/50 Rh atoms, where the atomic fractions represent probabilities.

In general, the structure factor of any unit cell is given by

$$|F(\vec{Q})|^2=|F_{\text{nuclear}}(\vec{Q})|^2+|F_{\text{magnetic}}(\vec{Q})|^2, \tag{A1}$$

with the nuclear contribution of

$$|F_{\text{nuclear}}(\vec{Q})|^2=\left|\sum_j b_j e^{i\vec{Q}\cdot\vec{r}_j}\right|^2 \tag{A2}$$

and the magnetic part of

$$|F_{\text{magnetic}}(\vec{Q})|^2=\left|\sum_j p_j(\hat{p}_j\times\hat{Q})e^{i\vec{Q}\cdot\vec{r}_j}\right|^2. \tag{A3}$$

The sums run over all atoms of the unit cell. b_j and p_j are the nuclear and magnetic scattering lengths of the jth atom. The unit vectors $\hat{p}_j$ and $\hat{Q}$ denote the directions of magnetic moment of the jth magnetic site and of the scattering vector $\vec{Q}$, respectively. $\vec{r}_j$ is the position vector of jth site with respect to the origin of the unit cell.

[1] S. N. Piramanayagam, J. Appl. Phys. **102**, 011301 (2007).
[2] D. A. Thompson and J. S. Best, IBM J. Res. Dev. **44**, 311 (2000).
[3] H. J. Richter and S. D. Harkness IV, MRS Bull. **31**, 384 (2006).
[4] S. Yuasa, H. Miyajima, and Y. Otani, J. Phys. Soc. Jpn. **63**, 3129 (1994).
[5] S. Yuasa, T. Akiyama, H. Miyajima, and Y. Otani, J. Phys. Soc. Jpn. **64**, 3978 (1995).
[6] K. Takizawa, T. Ono, and H. Miyajima, J. Magn. Magn. Mater. **226-230**, 572 (2001).
[7] S. Yuasa and H. Miyajima, Nucl. Instrum. Methods Phys. Res. B **76**, 71 (1993).
[8] P. A. Algarabel, M. R. Ibarra, C. Marquina, S. Yuasa, H. Miyajima, and Y. Otani, J. Appl. Phys. **79**, 4659 (1996).
[9] J. U. Thiele, L. Folks, M. F. Toney, and D. K. Weller, J. Appl. Phys. **84**, 5686 (1998).
[10] B. D. Cullity, *Elements of X-Ray Diffraction* (Addison-Wesley, Reading, MA, 1978).
[11] P. J. Brown, *International Tables for Crystallography C* (Kluwer, Dordrecht, 1992), p. 391.
[12] A. D. Krawitz, *Introduction to Diffraction in Materials Science and Engineering* (Wiley, New York, 2001).
[13] J. M. Cowley, *Diffraction Physics*, 2nd ed. (North-Holland Personal Library, Amsterdam, 1986).
[14] L. H. Schwartz and J. B. Cohen, *Diffraction from Materials* (Academic, New York, 1977).
[15] D. Richter, *Magnetism Goes Nano* (FZ Jülich GmbH, Jülich, 2005).
[16] G. Ehlers and F. Klose, *Handbook of Advanced Magnetic Materials*, Characterization and Simulation Vol. 2, edited by Yi Liu, D. J. Sellmyer, and Daisuke Shindo (Springer, New York, 2006), pp. 66–112.
[17] R. M. Moon, T. Riste, and W. C. Koehler, Phys. Rev. **181**, 920 (1969).
[18] V. L. Moruzzi and P. M. Marcus, Phys. Rev. B **46**, 14198 (1992).
[19] N. I. Kulikov, E. T. Kulatov, L. I. Vinokurova, and M. Partavi-Horvath, J. Phys. F: Met. Phys. **12**, L91 (1982).
[20] V. L. Moruzzi and P. M. Marcus, Phys. Rev. B **48**, 16106 (1993).
[21] J. U. Thiele, Matthias Buess, and Christian H. Back, Appl. Phys. Lett. **85**, 2857 (2004).
[22] Ganping Ju, Julius Hohlfeld, Bastiaan Bergman, Rene J. M. van de Veerdonk, Oleg N. Mryasov, Jai-Young Kim, Xiaowei Wu, Dieter Weller, and Bert Koopmans, Phys. Rev. Lett. **93**, 197403 (2004).
[23] O. N. Mryasov, U. Novak, K. Y. Guslienko, and R. W. Chantrell, Europhys. Lett. **69**, 805 (2005).
[24] O. N. Mryasov, J. Magn. Magn. Mater. **272-276**, 800 (2004).
[25] R. Skomski, J. Phys.: Condens. Matter **15**, R841 (2003); E. Tartakovskaya, Phys. Rev. B **71**, 180404(R) (2005); E. V. Tartakovskaya, J. W. Tucker, and B. A. Ivanov, J. Appl. Phys. **89**, 8348 (2001).
[26] H. B. Callen and E. Callen, J. Phys. Chem. Solids **27**, 1271 (1966).
[27] J. U. Thiele, K. R. Coffey, M. F. Toney, J. A. Hedstrom, and A. J. Kellock, J. Appl. Phys. **91**, 6595 (2002).
[28] S. Okamoto, N. Kikuchi, O. Kitakami, T. Miyazaki, Y. Shimada, and K. Fukamichi, Phys. Rev. B **66**, 024413 (2002).
[29] J. B. Staunton, L. Szunyogh, A. Buruzs, B. L. Gyorffy, S. Ostanin, and L. Udvardi, Phys. Rev. B **74**, 144411 (2006).
[30] R. Skomski, O. N. Mryasov, J. Zhou, and D. J. Sellmyer, J. Appl. Phys. **99**, 08E916 (2006).
[31] A. B. Shick and O. N. Mryasov, Phys. Rev. B **67**, 172407 (2003).
[32] G. Brown, B. Kraczek, A. Janotti, T. C. Schulthess, G. M. Stocks, and D. D. Johnson, Phys. Rev. B **68**, 052405 (2003).
[33] X. Wang, R. Wu, D. S. Wang, and A. J. Freeman, Phys. Rev. B **54**, 61 (1996).